

MHD Stability in X-point Geometry: Simulation of ELMs

G.T.A. Huysmans

Association Euratom-CEA, CEA/DSM/DRFC, Centre de Cadarache, 13108 St. Paul lez Durance, France

e-mail: guido.huysmans@cea.fr

Abstract A non-linear MHD code, named JOREK, is under development with the aim to study the non-linear evolution of the MHD instabilities thought to be responsible for Edge Localised Modes: external kink(peeling) and medium-n ballooning modes. The full toroidal X-point geometry is taken into account including the separatrix, open and closed field lines. Analysis of the influence of the separatrix shows a strong stabilisation of ideal and resistive MHD external kink/peeling modes. One instability remains unstable in the presence of the X-point, characterised by a combination of a tearing and a peeling mode. The so-called peeling-tearing mode shows a much weaker dependence on the edge q . Non-linearly the $n=1$ peeling-tearing mode saturates at a constant amplitude yielding a mostly kink-like perturbation of the boundary with an island-like structure close to the x-point. The non-linear evolution of a medium-n ballooning mode shows the formation of density filaments. The density filaments are sheared off from the main plasma by an $n=0$ flow non-linearly induced by the Maxwell stress. The amplitude of the ballooning mode is limited by this $n=0$ flow and multiple (in time) density filaments can develop to bring the plasma below the stability boundary.

1. Introduction

Edge localised modes (ELMs) associated with the edge transport barrier in H-mode plasmas remain an important issue for ITER. Extrapolating the size of the ELMs towards to the ITER collisionality leads to a very large predicted ELM size [1]. The resulting energy flux towards the first wall could be difficult to handle in ITER [2]. The estimations of the ELM size in ITER are based on extrapolation of current experiments. However, no convincing ELM model exists to indicate which are the appropriate parameters to use in the extrapolation. It is therefore essential to improve the understanding of the physical mechanism of ELMs.

It is generally accepted that the onset of an ELM is caused by MHD instabilities, notably ballooning modes driven by the edge pressure gradient and the external kink (peeling) modes driven by the edge bootstrap current. The linear ideal MHD instabilities have been studied in considerable detail and a good agreement is generally found between the observed pressure gradients and the ideal MHD stability limits. Medium-n so-called peeling/ballooning modes driven by both the pressure gradient and the current density are typically found to be the most relevant. However, even on the linear MHD stability limits questions remain, notably the influence of the x-point on the stability limit of the external kink (peeling) modes.

Much less established is the non-linear phase of the ELM. One important open question is what determines the amplitude of the ELM energy losses, i.e. how far can the plasma exceed the MHD stability limit and what determines the pressure gradient and current density after the ELM. The non-linear behaviour and relaxation mechanism of the external kink (peeling) and ballooning modes in the edge pedestal is still largely unknown. Analytic theory of the early non-linear phase suggests that the ballooning mode grows explosively [3] and leads to the formation of magnetic filaments. Indications of the explosive growth and filamentation have been observed in non-linear simulations of the rise phase of an unstable ballooning mode [4]. MHD simulations of the complete cycle of the ELM, starting from a stable plasma, through the MHD stability limit, up to the end of the relaxation, have not yet been published. In order to study the non-linear evolution of the ballooning and external kink modes in the correct tokamak geometry including the x-point/separatrix and the open field lines, the non-linear MHD code (named JOREK) is being developed [5].

This paper describes the first applications of the JOREK code to the evolution of the n=1 external kink mode and the medium-n ballooning modes. In section 2, a short description of the MHD model and the numerical method implemented in the JOREK code is given. Section 3 first discusses the stabilising influence of the separatrix on the stability of the $n=1$ external kink / peeling mode in both the ideal and the resistive MHD model, followed by the non-linear evolution of the remaining instability. In section 4 the results on the non-linear evolution of a single unstable medium-n ballooning mode are presented.

2. The non-linear MHD code JOREK

The MHD model implemented in the present version of the JOREK code is the reduced MHD model in toroidal geometry [6]. The poloidal flux, vorticity, density and temperature are evolved in time. The equations are solved in the weak form given below:

$$\begin{aligned}
 \vec{v}_\perp &= \frac{-R^2}{R_0 B_0} \nabla u \times \nabla \varphi & B &= R_0 B_0 \nabla \varphi + R_0 \nabla \psi \times \nabla \varphi & J &= \Delta^* \psi & w &= \nabla_\perp^2 u \\
 \int \rho^* \frac{\partial \rho}{\partial t} dV &= \int + \rho^* \rho \frac{2}{R_0 B_0} \partial_2 u + \rho^* \frac{R}{R_0 B_0} [\rho, u] - D_\perp \nabla \rho^* \cdot \nabla_\perp \rho + \rho^* S_\rho dV \\
 \int T^* \frac{\partial T}{\partial t} dV &= \int \left(+ \frac{2(\gamma-1)}{R_0 B_0} T^* T \partial_2 u + \frac{R}{R_0 B_0} T^* [T, u] - \nabla T^* \cdot (K_\perp \nabla_\perp T + K_\parallel \nabla_\parallel T) + T^* S_T \right) dV \\
 \int \psi^* \frac{R_0}{R^2} \frac{\partial \psi}{\partial t} dV &= - \int \nabla (\eta(T) \psi^*) \cdot \left(\frac{R_0}{R^2} \nabla_\perp \psi \right) dV - \int \psi^* \frac{1}{RB_0} [u, \psi] dV - \int \psi^* \frac{1}{R^2} \frac{\partial u}{\partial \phi} dV \\
 - \frac{1}{R_0 B_0} \int \nabla u^* \cdot \left(\hat{\rho} \frac{\partial \nabla_\perp u}{\partial t} \right) dV &= \int - \frac{1}{R} [u^*, \hat{\rho}] \frac{1}{2} v^2 dV - \hat{\rho} \frac{R}{R_0^2 B_0^2} [u^*, u] w dV + u^* \frac{R_0}{R} [\psi, j] dV \\
 \int -u^* \frac{R_0 B_0}{R^2} \partial_3 j dV + R [u^*, p] dV &- v(T) \nabla_\perp u^* \cdot \nabla_\perp w dV
 \end{aligned} \tag{1}$$

The boundary conditions correspond to those of an ideally conducting wall around the computational domain where all perturbations vanish.

The variables $[\psi, j, u, w, \rho, T]$ are discretised using generalised finite elements [7] in 3 dimensions. The generalised elements allow an arbitrary set of basis functions in each element so that the order of approximation can be adjusted on each element (so-called p-refinement). So far, the code is mostly used using linear finite elements in the poloidal plane and Fourier harmonics as the basis functions in the toroidal direction. The number of harmonics can in principle be adjusted at every grid point. The grid of finite elements can be locally refined at each time step by the subdivision of an element into two or four finite elements in the poloidal plane (h-refinement). To make use of any symmetry (N) in the solution (due to the choice of toroidal harmonics), the toroidal extent of the periodic grid can be reduced to $0 < \phi < 2\pi/(N-1)$. After the calculation of an equilibrium, the grid of finite elements is typically aligned to the flux surfaces inside and outside the separatrix. An example of a locally refined grid is shown in FIG. 1.

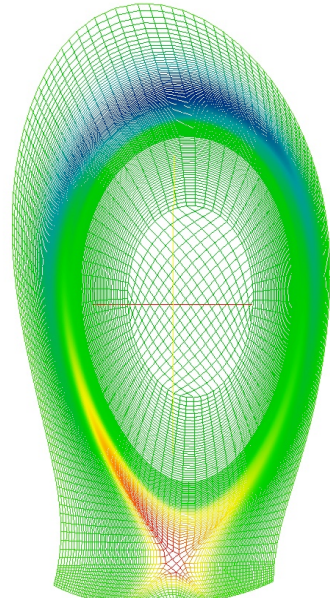


FIG. 1. Example finite element grid aligned on flux surfaces, locally refined at the separatrix. (color shows the equilibrium flow)

The time evolution scheme is fully implicit using the linearised Crank-Nicholson scheme:

$$\frac{\partial A(\vec{y})}{\partial t} = B(\vec{y}) \Rightarrow \left(\frac{\partial A(\vec{y}_n)}{\partial y} - \frac{1}{2}\delta t \frac{\partial B(\vec{y}_n)}{\partial y} \right) \delta \vec{y} = B(\vec{y}_n) \delta t \quad (2)$$

where the matrices A and B represent the (discretised) weak form of the equations (1). This leads to a large sparse matrix problem to be solved at every time step. The progress in the parallelised sparse matrix solvers, notably for general asymmetric matrices, is allowing the efficient solution of the single large matrix. Interfaces to the sparse matrix libraries MUMPS [8], WSMP [9] and PASTIX [10] are implemented. The fully implicit method allows large time steps, not limited by the size of the finite elements. The JOREK code is parallelised using MPI and through the use of the parallel sparse matrix solvers.

3. External kink (peeling) mode in X-point geometry

Ideal MHD external kink and peeling modes, driven unstable by the edge (bootstrap) current density in H-mode plasmas, are thought to be one of the relevant MHD instabilities in the onset or trigger of ELMs. The stability of kink and peeling modes is commonly evaluated using a plasma boundary truncated just inside the separatrix. This is necessary in MHD codes (like ELITE and MISHKA) that use a straight field line coordinate system to avoid the singular behaviour at the separatrix. This truncation changes the edge value of the safety factor q from infinity to a finite value. Ideal MHD peeling modes require the presence of a rational surface just outside the plasma to become unstable. While this is the case for truncated plasmas, in the presence of a separatrix all rational surfaces lie inside the plasma. This raises questions on the relevance of the peeling mode stability boundaries from truncated plasmas. Results from the ideal MHD KINX code [11], which does include the separatrix, shows a strong stabilisation of ideal MHD peeling modes. In the case of finite resistivity, resistive peeling modes, which do not require a rational surface outside the plasma, could become unstable.

The JOREK code, which includes the full plasma geometry including the separatrix and the open field lines, has been used to study the influence of the separatrix on the peeling mode stability. The well-established linear ideal/resistive MHD code CASTOR [12], using a truncated plasma boundary, is also used for comparison and benchmarking.

Using CASTOR with a plasma boundary closely approaching the separatrix, both the ideal and resistive MHD external kink/peeling modes when driven by the edge current gradient are found to be stabilised [13]. FIG. 2 shows the growth rate of the resistive external kink/peeling mode as a function of q on axis at a resistivity of $\eta = 2 \times 10^{-8}$ for several shapes of the boundary. The peeling mode resonant with q at the boundary is unstable ($q_0 \sim 1.7$) for the truncated boundary at $\psi_b = 0.99$ but is stable for $\psi_b = 0.998$ (CASTOR) and with the full separatrix (JOREK). There is a very good agreement between the CASTOR and JOREK code results. The fact that both ideal and

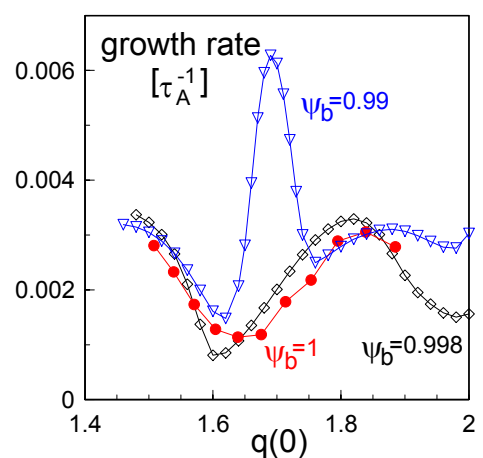


FIG. 2 The growth rate of the $n=1$ external kink mode as a function of q on axis with a boundary truncated at $\psi_b = 0.99$ (triangles) and $\psi_b = 0.998$ (diamonds) and with the separatrix $\psi_b = 1$ (circles).

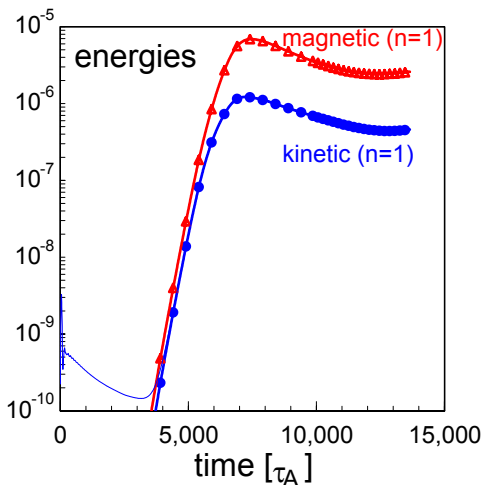


FIG. 3 Time evolution of the magnetic and kinetic energy of an $n=1$ peeling-tearing mode.

displacement close to the X-point. At the other poloidal location there is no phase change and the mode structure is kink-like. The stability boundary of the peeling-tearing mode as a function of the edge current density (at zero pressure gradient) is similar to the ideal MHD kink/peeling mode with a truncated plasma boundary. The dependence of the peeling-tearing mode stability limit on the edge pressure gradient has not yet been determined. However, the small growth rates of the peeling-tearing would make the mode sensitive to diamagnetic stabilisation.

The non-linear evolution of the $n=1$ peeling-tearing mode has been studied using the JOREK code. The starting equilibrium is unstable to the peeling-tearing mode due to a large edge current density ($J_{\text{ped}}/J(0) = 0.57$). This current is maintained by an applied axi-symmetric electric field that compensates the Ohmic dissipation.

After an initial linear phase of exponential growth ($\lambda \approx 8 \times 10^{-4} \tau_A^{-1}$), the mode saturates non-linearly into a steady state (see FIG. 3). The density profile in this phase is shown in FIG. 4. The boundary shows a kink-like perturbation except close to the X-point where the perturbation causes a local flattening of the density profile. This flattening moves as a function of the toroidal angle from inboard to outboard but remains localised close to the x-point. The structure in the central density profile is due an $m/n = 2/1$ island caused by an unstable tearing mode.

The saturation of the $n=1$ peeling-tearing mode is consistent with the observations of the so-called ‘Outer Mode’ in JET in Hot-Ion H-mode discharges. The Outer Modes occur mostly at low collisionality, i.e in the regime with large edge bootstrap currents. The Outer Modes can be long lived (\sim hundreds of ms) and are usually saturated at small amplitude. The Outer Modes had been identified as saturated ($n=1$) ideal MHD external kink modes [14]. The comparison of the

resistive modes are stabilised implies that it is not the fact that all rational surfaces lie inside the plasma that is the explanation for the stabilisation. The exact cause for the stabilisation is not clear; an analytic theory valid for the separatrix geometry is required.

From FIG. 2 it is clear that while the (edge-q) resonant external kink/peeling mode is stabilised by the separatrix, a resistive instability remains unstable. This instability does not show a strong dependence of the edge q values. The mode structure of the remaining instability shows features of both a tearing mode (at the resonant surface close to the boundary, $q = 4$ in this case) and of a peeling mode. This mode has been named peeling-tearing mode. The mode is characterised (at low resistivity) by a change of phase (as a function of radius) of the perpendicular

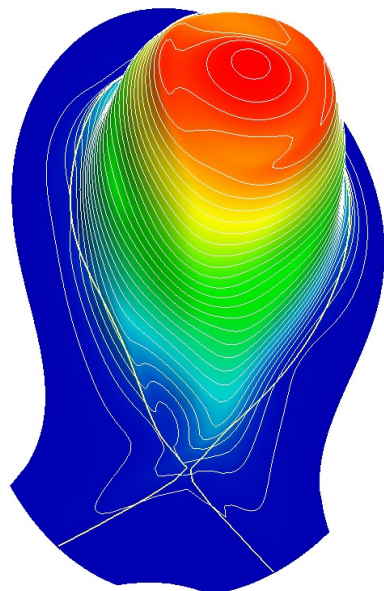


FIG 4 The density profile in the presence of a saturated $n=1$ peeling-tearing mode. Also shown is the separatrix.

mode structure with SXR measurements in [14] is based on ideal MHD external kink/peeling mode structure of a plasma with a truncated boundary. Given the strong stabilising influence on the separatrix and the fact that the mode structure of the peeling tearing mode is mostly kink-like, it seems more likely that the Outer Modes are better interpreted as peeling-tearing modes. However, a detailed comparison of the measurements with the non-linearly saturated state obtained with the JOREK code is needed to confirm this.

The peeling-tearing mode could also be relevant for the saturated MHD mode, the Edge Harmonic Oscillation (EHO), that stabilises ELMs in the so-called QH-mode regime [15]. The EHO is localised in the edge transport barrier with a dominant toroidal mode number of $n=1$. The electron temperature of EHO perturbation does not show a change of phase as a function of the radius in the mid-plane [16]. These features and the observed absence of a strong edge q dependence [17] are consistent with the peeling-tearing mode.

The low growth rate and the non-linear saturation suggest that the peeling-tearing mode is not likely to be directly responsible for the ELM crash. However the mode could play role as a trigger for the ballooning mode due to the toroidal asymmetry it induces. This could locally (as a function of toroidal angle) enhance the pressure gradient and destabilise a ballooning mode.

4. Non-linear evolution of medium-n ballooning modes

The most relevant MHD instabilities for the ELMs are the medium-n ideal MHD ballooning modes. High-n ballooning modes are the most easily stabilised by diamagnetic flow, toroidal flow or commonly the second stable regime. The low-n modes are more stable due to the field line bending. As a first approach to simulate a full ELM crash, the non-linear evolution of a $n=6$ ballooning mode has been studied using the JOREK code. The simulations typically start from an equilibrium unstable, but close to marginal stability, to medium-n ideal MHD ballooning mode. The initial equilibrium is characterised by a large pressure gradient at the separatrix. This gradient is maintained due to a local reduction of the density and temperature diffusivities ($D_{pedestal} = 0.1D_{\perp}$, $K_{pedestal} = 0.1K_{\perp}$, for $\psi/\psi_{sep} > 0.9$). The large gradients are causing a significant flow in the poloidal plane due to the finite resistivity (Pfirsch-Schluter flow). The equilibrium flow consists of two poloidally extended convective cells centered on the separatrix. One convective cell centered at the X-point, the other around the top of the plasma.

The evolution of the magnetic and kinetic energies of the $n=6$ ballooning mode and of the $n=0$ flow is shown in FIG. 5. Also shown is the volume integrated density and pressure inside the separatrix. For this case, the perpendicular diffusivities are $D_{\perp} = K_{\perp} = 10^{-5}$, the resistivity and viscosity on axis $\eta(0) = \nu(0) = 5 \times 10^{-6}$. In the linear phase, the mode grows exponentially from the noise level

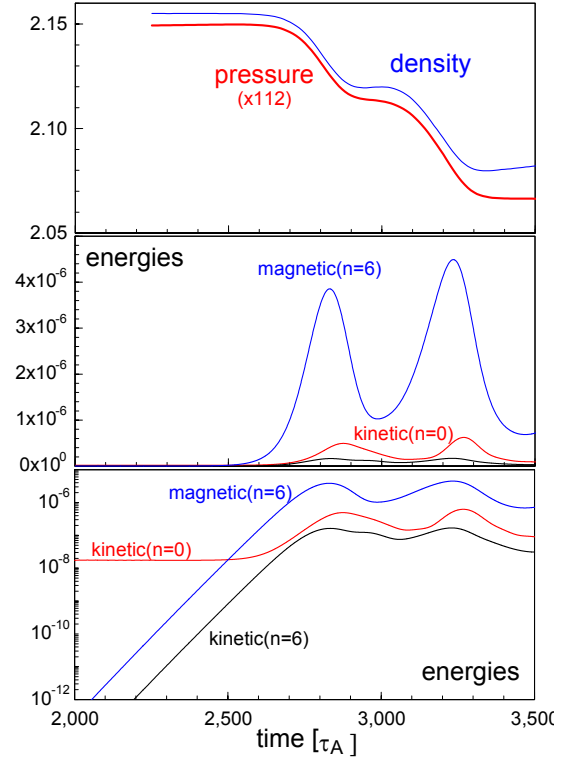


FIG. 5. The evolution of the total pressure and density (top) and magnetic and kinetic energy evolution of an $n=6$ ballooning mode and the $n=0$ kinetic energy.

with a linear growth rate of $0.011 \tau_A^{-1}$. Figure 6a show the streamlines of the total velocity due to the ballooning perturbation and the equilibrium flow at the end of the linear phase ($t = 2650 \tau_A^{-1}$). The asymmetry in the radial position of the convective cells on the outboard side is due to the ballooning mode flow which adds or subtracts from the equilibrium flow depending on the phase. Even though the magnetic energy perturbation is much larger than the kinetic perturbation, the perturbation to the flux surfaces remains small. The maximum radial displacement of the flux surfaces is about $\xi_\psi = 4 \times 10^{-3}$.

The non-linear phase is characterised by the excitation of a strong poloidal flow inside along the separatrix with toroidal and poloidal mode numbers $n=0, m=0$ resembling a zonal flow. The amplitude of the $n=0$ flow is much larger than the equilibrium flow and larger but comparable to the $n=6$ flow due to the ballooning mode. The induced $n=0$ flow strongly distorts the flow pattern of the ballooning mode.

In the early non-linear phase the density moves inward and outward at different poloidal angles following the flow pattern of the ballooning mode (see FIG. 6b). At a later stage the $n=0$ flow causes the low-density plasma to flow poloidally behind the high-density plasma. The result is that the high-density plasma is sheared off from the main plasma and forms a

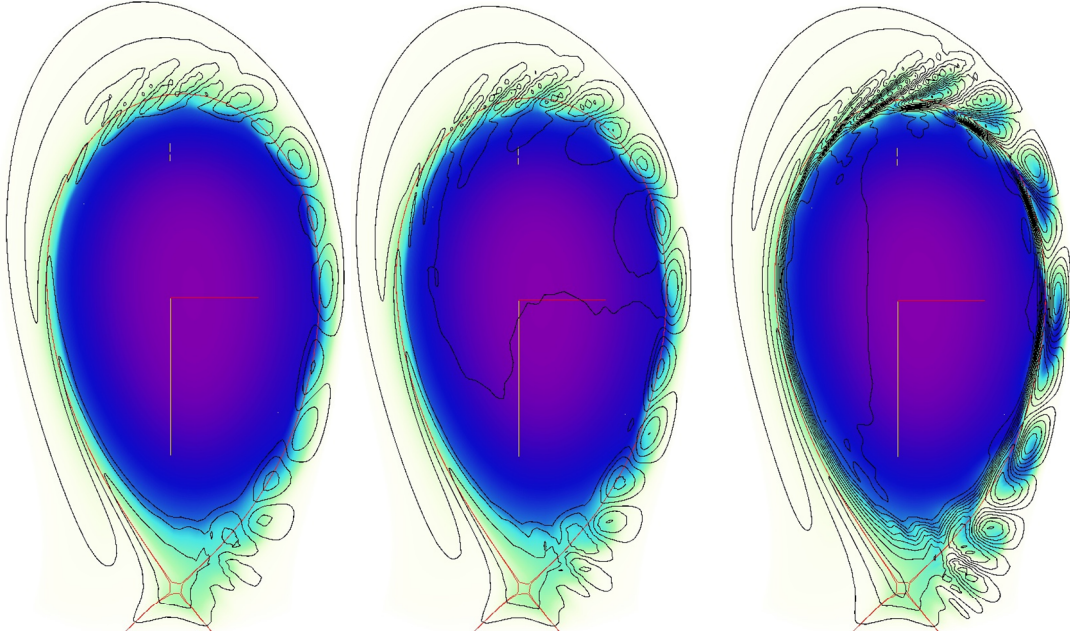


FIG. 6. The density and velocity streamlines at (a) $t = 2650 \tau_A^{-1}$, (b) $t = 2700 \tau_A^{-1}$ and (c) $t = 2890 \tau_A^{-1}$ due to an $n=6$ ballooning mode.

high density ‘blob’ or filament (see FIG. 6c). These density filaments are aligned to the field lines and exist only on the low-field side. After the blob formation the $n=6$ ballooning mode and the $n=0$ flow decay.

The saturation of the ballooning mode is caused by the induced $n=0$ ‘zonal’ flow. When the $n=0$ flow has decayed, the ballooning mode starts to grow again. Subsequently, also the $n=0$ is driven again and causes another set of density filaments to be sheared off the plasma. This indicates that the plasma is not yet stable to the ballooning mode after the first event. The total number of bursts of the ballooning mode depends on how far the initial equilibrium was above the MHD stability limit. For an initial equilibrium very close to marginal stability one burst can be enough to make the plasma stable. In this case the saturation of the ballooning mode is probably due to both the $n=0$ flow and the reduction of the ballooning mode drive (i.e. the pressure gradient).

The non-linear drive of the $n=0$ flow is due to the $[\psi_n, J_n]$ non-linearity (Maxwell stress) in the momentum equation. With the growth of the ballooning mode, the 2D equilibrium balance

$\nabla p \approx J \times B$ changes to a (near) balance between the terms $\partial J / \partial \varphi$, $[\psi, J]$, ∇p and the viscosity (see FIG. 7a). In the $n=0$ component of the momentum equation the imbalance between the terms $[\psi_0, J_0]$, ∇p , $[\psi_n, J_{-n}]$ and the viscosity drives the $n=0$ flow. This imbalance in the $n=0$ component is rather small: 2 to 4 orders smaller than the equilibrium terms. The Reynolds stress terms (the non-linearities in velocity), which drive the zonal flow in electrostatic turbulence, are small (see FIG. 7b).

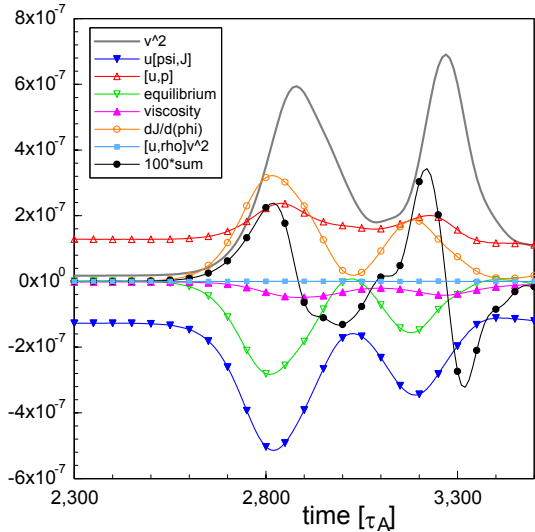


FIG. 7a The time evolution of the contributions to the total kinetic energy.

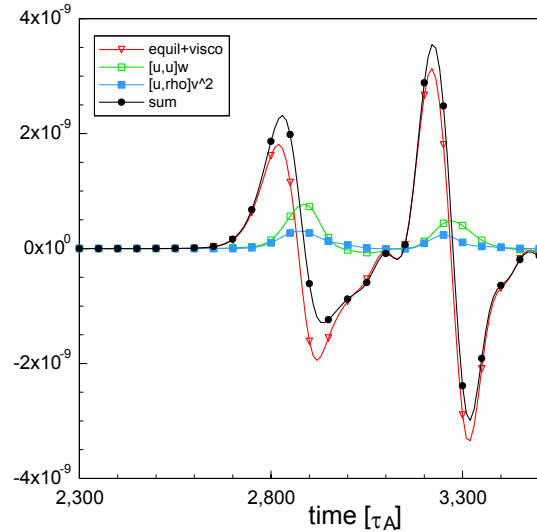


FIG. 7b The evolution of the terms in the $n=0$ component of the kinetic energy.

The blobs do not appear to have an obvious magnetic structure. Due to the large heat conduction along the field lines, the temperature of the blobs is similar to the background temperature. The profiles of the density, temperature and poloidal flow component as a function of radius in the mid-plane are shown in FIG. 8. The density profiles clearly show the combined effect of the ballooning mode and the non-linearly driven $n=0$ flow: The high-density plasma has moved outwards with low-density plasma moving behind it from a different poloidal angle. The resulting density profiles are very similar to those measured during ELMs in MAST [18]. The temperature only shows a very small increase at the position of the density blob.

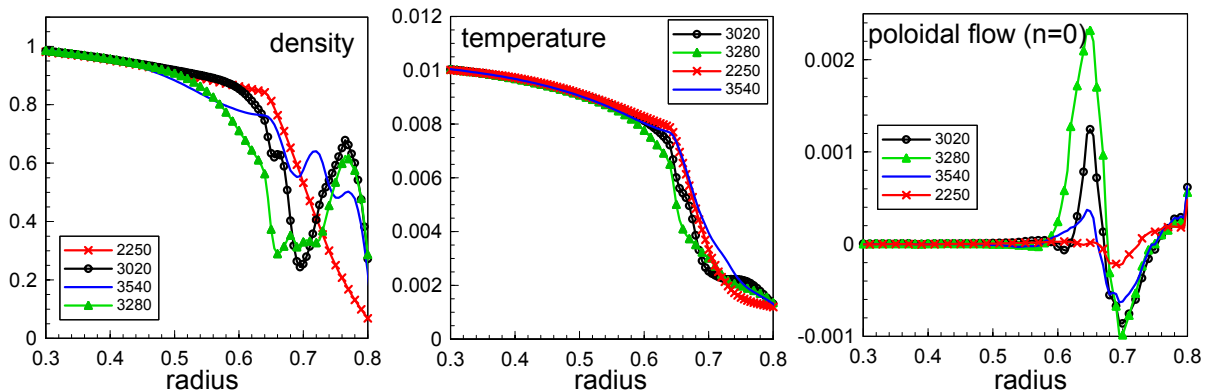


FIG. 8 Profiles of the density, temperature and poloidal flow velocity as a function of radius in the outboard mid-plane at several time slices.

5. Conclusions

The non-linear evolution of the MHD instabilities relevant for the ELMs, external-kink (peeling) modes and medium-n ballooning modes have been studied using the non-linear MHD code JOREK. The linear ideal and resistive external-kink (peeling) modes are found to be strongly stabilised by the presence of the separatrix. The remaining resistive instability (named peeling-tearing mode) shows features of both external kink and tearing. Non-linearly, this instability saturates into a steady state with the plasma boundary deformed with a kink-like perturbation and an island-like structure close to the x-point.

The medium-n ballooning mode develops ‘blobs’ or density filaments in the non-linear phase. The density follows the streamlines of the $E \times B$ velocity. A strong $n = 0, m = 0$ flow is driven by the $[\psi, J]$ non-linearity (Maxwell stress) leading to a flow of low-density plasma behind the high density flowing outwards. This shears the density filaments off the main plasma with a ‘depression’ in the density behind the filaments. In the present simulations, these density filaments do not appear to have an obvious magnetic structure. The maximum amplitude of the ballooning mode is limited by the $n = 0$ flow, leading to multiple (in time) filaments until the plasma is stable.

References

- [1] A. Loarte et al., Physics of Plasmas, Vol. 11, No. 5 (2004) 2668
- [2] G. Federici et al., Plasma Physics Control. Fusion, **45** (2003) 1523
- [3] H.R. Wilson and S. Cowley, PRL Vol. 92, No. 17, (2004) 175006-1
- [4] P.B. Snyder, H.R. Wilson and X.Q. Xu, Phys. Plasmas **12**, 056115, 2005
- [5] G.T.A. Huysmans et al., Theory of Fusion Plasmas: Proceedings of the Joint Varenna-Lausanne International Workshop, Varenna, 2002
- [6] Briguglio, Zonca and Vlad, Phys. Plasmas Vol.5 No.9 (1998)
- [7] I. Babuska and J.M Melenk, International Journal for Numerical Methods in Engineering 40, 727-758, (1997)
C.A.M. Duarte and T.J. Oden, Computer Methos in Applied Mechanics and Engineering, 139, 237-262, (1996)
- [8] J.T. Oden, C.A. Duarte and O.C. Zienkiewicz, Computer Methods in Applied Mechanics and Engineering, 153, 117-126, (1998)
- [9] P. R. Amestoy, I. S. Duff and J-Y. L'Excellent, in Comput. Methods in Appl. Mech. Eng., 184, pp 501-520 (2000)
P. R. Amestoy, I. S. Duff, J. Koster and J.-Y. L'Excellent, SIAM Journal of Matrix Analysis and Applications, Vol 23, No 1, pp 15-41 (2001)
- [10] A. Gupta, G. Karypis, and V. Kumar. Highly scalable parallel algorithms for sparse matrix factorization. IEEE Transactions on Parallel and Distributed Systems, 8(5):502–520, May 1997
- [11] P. Hénon, P. Ramet, and J. Roman, Parallel Comput. 28, 2 (Feb. 2002), 301-321
- [12] S. Yu. Medvedev et al., Plasma Phys. Control. Fusion **48** (2006) 927–938
- [13] W. Kerner et al., 1998 J. Comput. Phys. **142** 271–303
- [14] G.T.A. Huysmans, Plasma Phys. Control. Fusion **47** (2005) 2107–2121
- [15] G.T.A. Huysmans., T. Hender and B. Alper 1998 Nucl. Fusion **38** 179
- [16] Burrell K.H. et al 2002 Plasma Phys. Control. Fusion **44** A253
- [17] W. Suttrop et al., Nucl. Fusion **45** (2005) 721–730
- [18] W. Suttrop et al., Plasma Phys. Control. Fusion **46** (2004) A151–A156
- [19] A. Kirk et al., PRL **96**, 185001 (2006)